PHYSICAL REVIEW A VOLUME 22, NUMBER 3 SEPTEMBER 1980

Effects of electric fields on doubly excited autoionizing Rydberg states of barium

K. A. Safinya, J. F. Delpech,* and T. F. Gallagher
Molecular Physics Laboratory, SRI International, Menlo Park, California 94025
(Received 19 February 1980)

We report the effects of static electric fields on the doubly excited $6p_{1/2}nl$ states of barium in the region $n^* = 12$. Using a three-step laser excitation scheme we have measured the electric-field dependence of the positions and autoionization widths of the $6p_{1/2}$-$17s$, $16p$, $15d$, $12l$ ($l = 4$–10), $12f$, and $16s$ states at field values of up to 4.92 kV/cm. The photoexcitation spectra of the autoionizing states exhibit interference effects which are well understood and provide a better understanding of the character of these states in electric fields. The systematic study of the spectra and positions allows us to explain the field dependence of the autoionization widths in terms of electric-field mixing of the discrete portions of the autoionizing states. The relationship of these effects to dielectronic recombination rates of ions and electrons in plasma microfields is discussed.

I. INTRODUCTION

The experimental study of bound Rydberg states in static electric fields has received a great deal of attention in previous years. Of particular note is the extensive work by Zimmerman *et al.*[1] on the Stark structure of most alkali metals and the investigation of Zimmerman *et al.*[2] of the Stark structure of the bound Rydberg states of Ba around $n^* = 12$. The effects of electric fields on quasibound *autoionizing* Rydberg states, however, have not received the same attention as the bound Rydberg states mentioned above. Autoionizing Rydberg states are physically interesting since they are a discrete set of states embedded in a continuum of states. An electric field will not only affect the coupling between the discrete parts of the states, analogous to bound Rydberg state behavior in electric fields, it may also change the coupling between the discrete and continuum parts of the states. In the first experimental observation of electric-field effects on the autoionizing states of Sr, Freeman and Bjorklund[3] reported that the shapes and widths of the autoionizing resonances could be strongly influenced by electric fields. They suggested that the variations in the observed line shapes were due to the influence of the electric field on the bound portion of the autoionizing states.

In this work we have extended our investigations of doubly excited Rydberg autoionizing states of Ba to the region of nonzero electric field. Specifically, we have mapped out the doubly excited states of barium with a $6p_{1/2}$ core between 678 and 797 cm^{-1} below the $6p_{1/2}$ ionization limit in electric fields of up to 4.92 kV/cm. This corresponds to the effective quantum number n^* of the Rydberg electron ranging from about 11.7 to 12.7. In addition, we have measured the widths of these states as a function of the electric field. Since the range of states studied constitutes one complete n cycle we were able to observe a wide variety of spectra which are described in Sec. III. This study is of particular interest because of the close relationship between autoionization of doubly excited Rydberg states and dielectronic recombination of ions and electrons in plasmas.[4] The detailed experimental study of the electric-field effects on Rydberg autoionizing states is vital to an understanding of microfield effects on dielectronic recombination rates in plasmas. This relationship is discussed in detail in the Appendix.

Included in this work are the higher angular-momentum states of the $n=12$ hydrogenic manifold which exhibit field-independent widths in the linear Stark region, as expected from the model discussed in the Appendix. We have also observed field varying line shapes and widths of nonhydrogenic levels which are not inconsistent with the earlier observations of Freeman and Bjorklund.[3]

In Sec. II we describe the experiment and the technique used. In Sec. III we present the experimental results and discuss the positions and widths of the different states observed. In this section we attempt to explain, by simple physical arguments, the various line shapes observed and the effects of electric field mixing on the autoionization widths of the states. In Sec. IV we conclude with a brief discussion and summary of the main findings of this work.

II. EXPERIMENT

The experimental technique is similar to the methods we have used previously[5] in studying autoionizing states of alkaline earths and is depicted by the level diagram in Fig. 1. The first two dye lasers at 5535 and ~4300 Å excite Ba atoms in an atomic beam from the $6s^2$ ground state to the $6s6p$ state, and then to a bound Rydberg Stark (RS) state $6s12k$. The third laser at ~4935 Å drives the transition to the autoionizing $6p_{1/2}12k$ RS state, which yields an ion which we detect. Only when

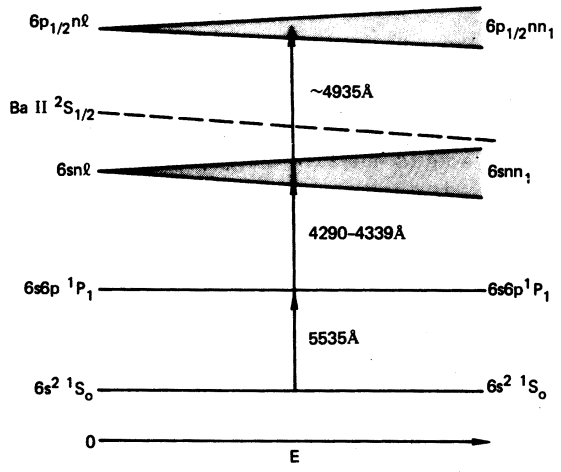

FIG. 1. Level diagram of Ba as a function of electric field E showing three-step laser excitation scheme used. The figure is not drawn to scale. The dashed line represents the first ionization limit of Ba.

the third laser is tuned to the $6s12k \rightarrow 6p12k$ resonance do we see an ion signal, and from the frequency and width of the resonance we can determine immediately the energy and autoionization rate of the $6p_{1/2}12k$ state.

A schematic drawing of the experimental apparatus is shown in Fig. 2. A collimated barium beam passed between a pair of stainless steel plates 1.22 cm apart used to apply the electric field. The three laser beams were roughly colinear and intersected the atomic beam at right angles, into the plane of the paper in Fig. 2. The ions produced by the autoionizing transition were swept into the multiplier through a Ni mesh in the top plate by the electric field. The output of the multiplier was amplified and fed into a boxcar averager gated by the laser trigger pulse. The voltages applied to the two plates were opposite in sign and equal in magnitude to keep the atomic beam at about ground potential. This balanced voltage configuration reduced the change in the time of flight of the Ba^+ ions as a function of the applied electric field and allowed us to leave the boxcar gate position fixed throughout the experiment, with one exception. The exception was when the dc field was equal to zero. In this case the Ba^+ ions were swept into the multiplier by applying a 1.5-kV positive pulse to the bottom plate roughly 3 μs after autoionization, in which case the boxcar gate had to be delayed by ~3 μs.

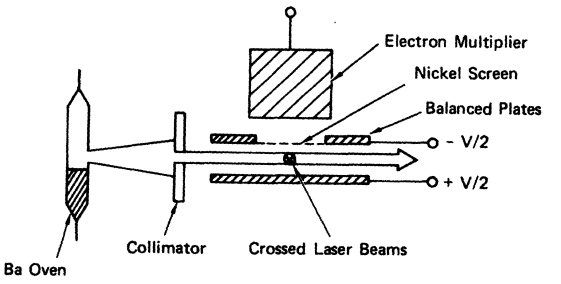

FIG. 2. Schematic diagram of beam apparatus.

The first part of the experiment involved the mapping out of the bound RS structure of Ba around $n^* = 12$, essentially reproducing the Stark state map of Zimmerman *et al.*[2] by a different technique. The electric field was set at a particular value and kept on at all times. The mapping out of the bound Stark states was a simple two-step process: The first step was the excitation to a bound RS state; the second step was the detection of that state by driving the autoionizing $6s \rightarrow 6p_{1/2}$ Ba core transition and detecting the Ba^+ ions produced due to autoionization. In step one Ba atoms were excited in an electric field to the bound Rydberg states by two fast pulse dye lasers at 5535 and roughly 4310 Å (see Fig. 1). These two lasers overlapped in space and time. In the second step, a third dye laser was spatially overlapped with the first two, but temporally delayed from them by 10 ns, and served to produce Ba^+ ions by driving the $6s \rightarrow 6p_{1/2}$ autoionizing core transition of Ba. The positions of the Ba resonance transition at 5535 Å and the autoionizing $6s \rightarrow 6p_{1/2}$ transition at ~4935 Å are insensitive to the electric fields that were applied here ($E_{max} = 4.92$ kV/cm. Also, because of their large oscillator strengths, these transitions were saturated by the lasers. Therefore, we were able to set the first and third dye laser wavelengths fixed at all field values and merely sweep the wavelength of the second laser to get the desired map of the bound RS states as a function of electric field. The wavelength of the second laser was swept from ~4290 to 4330 Å, covering the states (in zero field) from $6s17s$ to $6s14d$.

With the bound RS levels identified, the Stark structure of Ba with the $6p_{1/2}$ core was obtained by simply altering our experimental procedure. As before, the electric field was set at a particular value; however, now with the aid of the bound state map, the wavelength of the second laser was selected so as to populate a particular bound RS level. Then the wavelength of the third autoionizing laser was swept to produce the spectrum of the $6p_{1/2}$ core RS level. The map of the $6p_{1/2}$ core RS level was thus obtained by setting the second laser wavelength to the different bound RS levels and sweeping the third laser wavelength for different values of the electric field. In this way the positions and widths of the autoionizing states as a function of electric field were obtained. The wavelength of the third laser was calibrated by

populating a high Rydberg state near the first ionization limit of Ba in zero field and sweeping the third laser. The line center of the autoionizing state was used as the wavelength of the Ba^+ $6s \rightarrow 6p_{1/2}$ transition. The third laser wavelength was then calibrated relative to the Ba^+ ion line by using a 2-mm quartz etalon with a free spectral range (FSR) of 1.7 cm^{-1}. The laser linewidth was $\lesssim 0.4$ cm^{-1} and was therefore adequate for the linewidth measurements presented below.

III. RESULTS

The discussion presented in the first section describes a simple physical system to be studied. The results of the experiment show that although the simple physical picture of a set of Stark-shifted Rydberg levels with an excited $6p_{1/2}$ core is basically correct, one must also be aware of many subtle effects which complicate the picture and also make it more interesting. The spectra obtained in sweeping the wavelength of the autoionizing laser in zero-field experiments[6] generally show symmetric features with possible satellites. Recall that since the Rydberg electron is in a large orbit about the core electron, we may treat its state as independent of the core electron state. In this approximation, the autoionizing spectrum corresponds to the core electron making a strong dipole transition, basically the Ba^+ $6s \rightarrow 6p$ transition, with the Rydberg electron slightly readjusting its orbit. This approximation has been shown to be valid in cases where configuration mixing is small and where the presence of any satellites in the spectrum usually indicates an overlap between the Rydberg wave function with a ground-state core and Rydberg wave functions with an excited core.[6] In this experiment the same model applies, except that now the Rydberg states are mixed with each other and show satellites of different varieties.

The different types of spectra can be classified as follows: (i) symmetric lines with no satellites; (ii) satellites that show clear evidence of interference effects between two discrete autoionizing states (bound parts of the states are interfering), producing asymmetric Beutler-Fano profiles similar to our earlier observations[7]; (iii) satellites that show no interference effects but appear as symmetric lines appearing in the wings of the main transition being studied; (iv) satellites that are Beutler-Fano profiles due to interference between the direct photoionization excitation and the excitation to a discrete autoionizing state, characteristic of the more conventional Beutler-Fano excitations observed in single-photon-absorption spectroscopy.[8] In almost all cases, the satellites are identified. In fact, complications arise only for the p and d states, where the effects of spin complicate the spectra. However, the Stark structure of the main features can be extracted from the data with minimal effort. In addition, we were able to measure the widths of most of the states as a function of the electric field. We will first discuss the position of the excited-core states and will follow later with the results of the width measurements.

Figures 3(a) and 3(b) summarize the position measurements of the excited-core states around $n^* = 12$ in the electric field E. In Figure 3(a), we present the raw data, indicating the energy W, relative to the Ba^+ $6p_{1/2}$ limit of these states. At any particular value of E, the points in this map correspond to the centers of the main features observed in the photoexcitation spectra of the autoionizing states discussed above. Each state is represented by a symbol defined in Fig. 3(a). We have used zero field labels to identify the states. In all cases the three lasers were polarized along the electric direction. Since the initial state of the system is $^1S_0$ all the states in this map are $m_J = 0$ states. Figure 3(b) is a simplified version of Fig. 3(a) with lines drawn to show the state positions in a more conventional manner. This figure is intended to aid the reader to interpret Fig. 3(a) and should not be used to extract the state position. The symbols in Fig. 3(b) correspond to the same symbols in Fig. 3(a) and merely serve to identify the lines. In addition, we have labeled the lines with the zero field angular-momentum values (S, P, D, F) of the states for easy reference in the discussion that follows. In the discussion of this map we will systematically examine the different states observed. Since all of the spectra discussed are photoexcitation spectra from a bound RS state to an autoionizing RS state, "initial" and "final" states will refer to the initial and final states in this excitation. We will generally refer to the states by their field-free labels for the sake of simplicity; however, we also use the parabolic quantum number n_1 defined by Bethe and Salpeter.[9]

s states. These states showed normal symmetric spectra and did not mix with the hydrogenic manifolds, as can be seen by the insensitivity of their energies to the electric field. Since the initial state in the autoionizing excitation was $^1S_0$, the final state observed at zero field must be $(6p_{1/2}ns_{1/2})J=1$, $m_J = 0$ for both $n = 16$ and 17. Figure 4 shows a typical spectrum of the $6p_{1/2}16s_{1/2})J=1$ state at 2.46 kV/cm.

p and d states. Here the effects of spin become important and complicate the p and d spectra. As can be seen from Fig. 3, the spacing between the

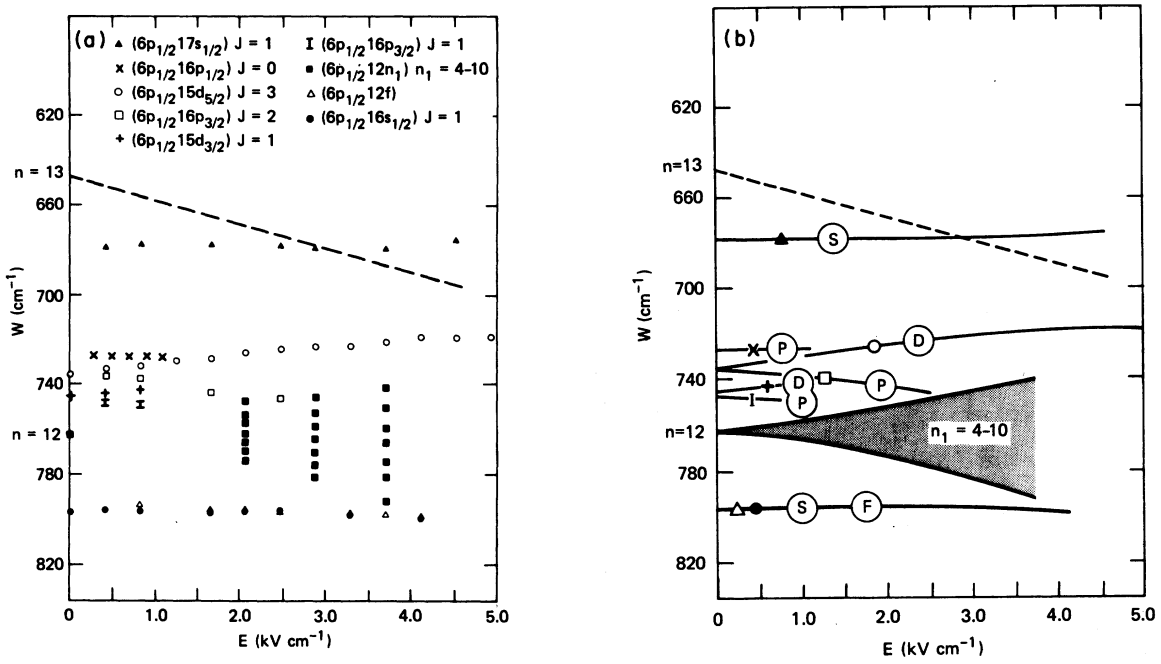

FIG. 3. Stark map of $6p_{1/2}nk$ autoionizing states showing the main features of the autoionization spectra. The energy scale is relative to the Ba^+ $6p_{1/2}$ limit. (a) The raw data. The position W of each state relative to the Ba^+ $6p_{1/2}$ limit is plotted for different values of the electric field E. We have used one symbol for each state as we plot its position versus E. The key to the symbols identifying the states is given in the upper portion of the figure. (b) This figure is drawn to aid the reader with (a). The solid lines were drawn through the points in (a); each line is identified by the corresponding symbol as defined above. The $n=12, n_1=4-10$ states are represented by the shaded area. The dashed line represents the $6p13f$ state.

three J components of the p state are roughly equal. This indicates that even though the spin of the inner $6p$ electron is coupled to its orbit (the $6p_{1/2}$-$6p_{3/2}$ splitting is roughly 1690 cm^{-1}), the spin-orbit coupling of the $16p$ electron is comparable to the Coulomb repulsion between the two electrons and, therefore, the zero-field states are neither jj coupled nor LS coupled, but are somewhere in between (intermediate coupling). The tentative assignments of the total J values for these states were made by populating the $6s_{1/2}16p$ states using the Stark switching technique originally suggested by Freeman and Kleppler[10] and used previously to populate higher l states of Sr,[6] and exciting the autoionizing transitions in zero field. Here the bound $6s16p$ states were populated in a field of ~80 V/cm; the field was turned off ($E<3$ V/cm) in 10 ns, 20 ns after the first two dye lasers were fired. The third laser was then fired 30 ns after the field had dropped to ~5% of its maximum value. By polarizing the third laser either along the polarizations of the first two lasers or perpendicular to it and by observing the changes in the resulting spectra, we were able to identify the various J states of the $6p_{1/2}16p$ manifold. In the presence of the dc electric field the $16p$ and $15d$ states show a strong mixing as expected. The mixing manifests itself both in the observed repulsion in Fig. 3 of the $(6p_{1/2}16p_{3/2})J=2$ state from the $(6p_{1/2}15d_{5/2})J=3$ state and in the core excitation spectra in Fig. 5 which were observed when the bound Rydberg state populated by the second laser was $(6s15d)^1D$, $(6s15d)^3D$, $(6s16p)^1P$, and $(6s16p)^3P$, respectively, at 820 V/cm.

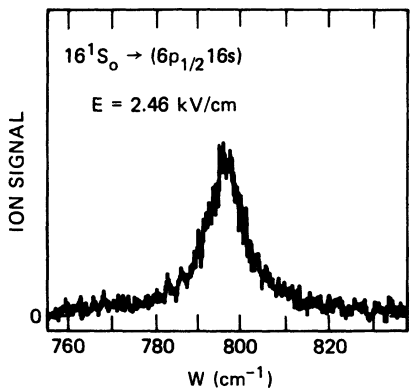

FIG. 4. Typical spectrum obtained for $6s16s\,^1S_0 \rightarrow (6p_{1/2}16s)J=1$ (zero-field state labels) showing symmetric behavior.

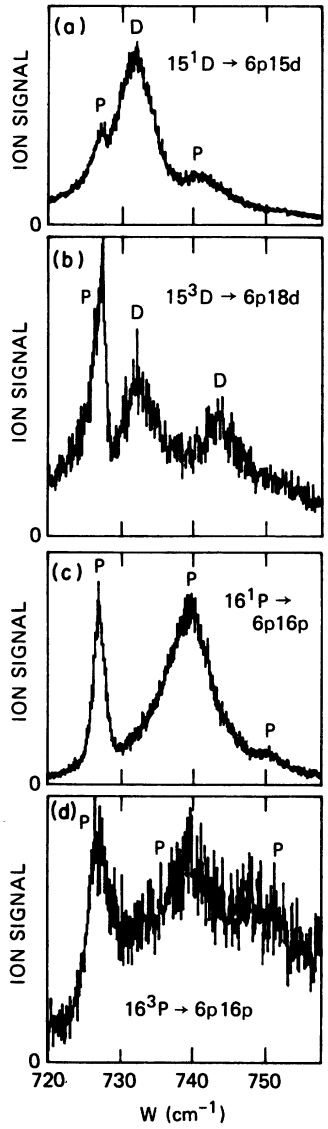

FIG. 5. Photoexcitation spectra for p and d autoionization transition at an electric field of 820 V/cm showing the ion signal as the third laser wavelength is swept. (a), (b), (c), and (d) correspond to the initial states $(6s15d)^1D$, $(6s15d)^3D$, $(6s16p)^1P$, and $(6s16p)^3P$ respectively, of the excitation. The satellites in each of the spectra show strong electric-field mixing of the p and d states.

In all four cases in Fig. 5 the sharp p state at $W \sim 727$ cm^{-1} is visible. When the initial state in the excitation is ^1D [Fig. 5(a)], we observe one large peak corresponding to the $(6p_{1/2}15d_{5/2})J=3$ (zero field) state and two smaller peaks which we identify as p states. Zero-field scans of this spectrum indicate that the $(6p_{1/2}15d_{3/2})J=1$ level is also excited, however, the peak height is $\lesssim 6\%$ of the main peak. The spectrum obtained when the initial state in the excitation was ^3D [Fig. 5(b)] clearly shows an interference between the bound portions of the p and d states at $W \sim 727$ cm^{-1} similar to interference effects observed previously.[7] The other two components in this spectrum were identified as $(6p_{1/2}15d_{5/2})J=3$ and $(6p_{1/2}15d_{3/2})J=1$. This was done in zero field, where p state mixing is absent, with the light from all three lasers circularly polarized. The resulting spectrum showed only one symmetric peak, which was identified as the $J=3$, $m_J=3$ component of the $6p_{1/2}15d_{5/2}$ state, since the ground state of Ba is $^1S_0$. When the polarization of all lasers was vertical, as was the case throughout most of the experiment, the zero-field spectrum showed an additional peak to the red side of the previously identified $J=3$ component. This second peak must be due to a $J=1$ state, since the final states reached by the lasers must have J odd. The splitting between those two states is ~ 11 cm^{-1}, which we attribute to the $1/r_{12}$ interaction since a splitting of this size is much too large to be due to the spin-orbit interaction for the $15d$ electron.

Figure 5(c) shows three main p components; the center feature is seen to be asymmetric with unresolvable structure to its blue side. This could either be the $15d$ state or another p state. The spectrum of Fig. 5(d) shows the same three p states with considerable loss in signal to noise. This is because the initial state in the excitation is ^3P and more difficult to populate. Here the signal to noise is too low to make any meaningul statements about d-state mixing. We see, however, that whether the initial state in the excitation is ^1P or ^3P, the final states reached are the same. This is also true of the d states. Thus the electron spins appear to be decoupled in some sense, with the inner electron in the $6p_{1/2}$ state. The similarities between Figs. 5(a) and 5(c), and 5(b) and 5(d) with regard to the ratios of the different peaks, however, suggest that the spins may not be completely decoupled.

f state. The effects of spin here are not important. One striking feature here is that the f state with an excited $6p_{1/2}$ core is substantially depressed in energy from its value with a smaller $6s_{1/2}$ core; the quantum defect of the f states has almost tripled. In fact, the changes in quantum defect for the observed Rydberg states are all positive (δ final $>\delta$ initial) and increase with increasing angular momentum for $l \lesssim 4$. Table I shows this effect for the s, p, d, and f states observed. The f state also mixes quite appreciably with the higher angular-momentum states from the $n=12$ manifold. Figure 6 shows the excitation spectrum of this state at 4.10 kV/cm showing very strong discrete state interference effects[7] which also

TABLE I. Quantum defects of barium Rydberg states with 6s and 6p cores.

	$\delta(6s$ core)[a]	$\delta(6p$ core)	$\Delta\delta$
16s	4.19	4.27(1)	+0.08(1)
16p	3.67	3.74(1)	+0.07(1)
15d	2.64	2.78(1)	+0.14(1)
12f	0.087	0.27(1)	+0.18(1)

[a] See Refs. 2 and 11.

affect the width of the f state as discussed below.

$n=12$, $10 \geq n_1 \geq 4$ states. These states appear to be well described by the linear Stark effect approximation using hydrogenic states and are typically positioned ± 2 cm^{-1} around the Ba$^+$ $6s \rightarrow 6p_{1/2}$ ion line.

In concluding the discussion of the map of Fig. 3, we wish to note a feature which is not present in Fig. 3. This is the absence of the $5d7d$ perturber, which is present in the bound-state spectrum of the Ba Rydberg Stark states at ~830 cm^{-1} below the first ionization limit of Ba.[2] When this state is initially populated, the photoexcitation spectrum obtained as the third laser swept is shown in Fig. 7. We see two peaks at the positions of the $(6p_{1/2}15d)$ and $(6p_{1/2}14d)$ states. The widths of the $5d7d \rightarrow 6p14d$ and $6s14d \rightarrow 6p14d$ transitions were measured as a function of laser power and found to show roughly equal values as a function of the laser power. This means that the character of the $5d7d$ state is mainly $^1D_2$. This designation agrees with the assignment made by Zimmerman *et al.*[2] and disagrees with the assignment of $^3F_2$ of Rubbmark *et al.*[11] An interesting feature of the spectrum of Fig. 7 is the shape of the $15d$ resonance. This Beutler-Fano profile shows clear evidence of interference of the discrete part of the state with the direct photoionization amplitude with an estimated Fano q parameter of 9(2). This means that the transition to the $6p15d$ state from the $5d7d$ state is roughly 130 times more likely

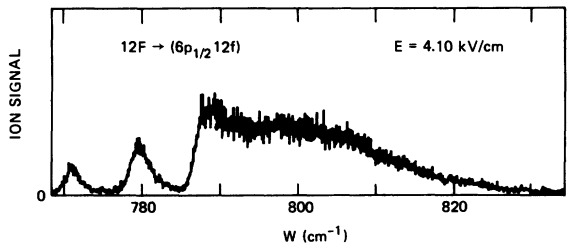

FIG. 6. $(6s12f)^1F \rightarrow (6p_{1/2}12f)$ (zero-field labels) photoexcitation spectrum at $E=4.10$ kV/cm showing interference between the discrete portions of the F state at the higher angular-momentum states from the $n=12$ manifold.

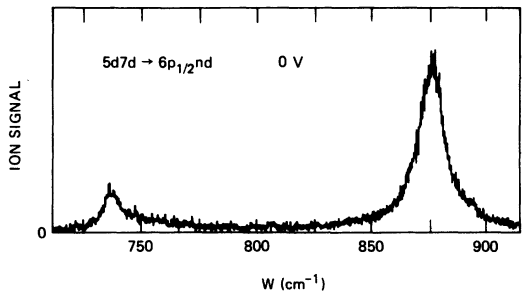

FIG. 7. Photoexcitation spectrum of the $5d7d$ perturber in zero field. The first two dye lasers populate the $5d7d$ state at $W \sim 830$ cm^{-1} below the Ba $\Pi^2S_{1/2}$ limit; the ion signal is recorded as the third laser wavelength is swept. The two peaks in the spectrum occur at the positions of the $(6p_{1/2}15d)^1D_2$ and $(6p_{1/2}14d)^1D_2$ states, suggesting that the $5d7d$ state should be designated $^1D_2$. The asymmetric profile at the position of the $15d$ state indicates an interference between the autoionization and direct photoionization amplitudes.

than direct photoionization to the continuum in a bandwidth equal to the autoionization width of the $6p15d$ state.

Figure 8 shows a plot of the widths of the

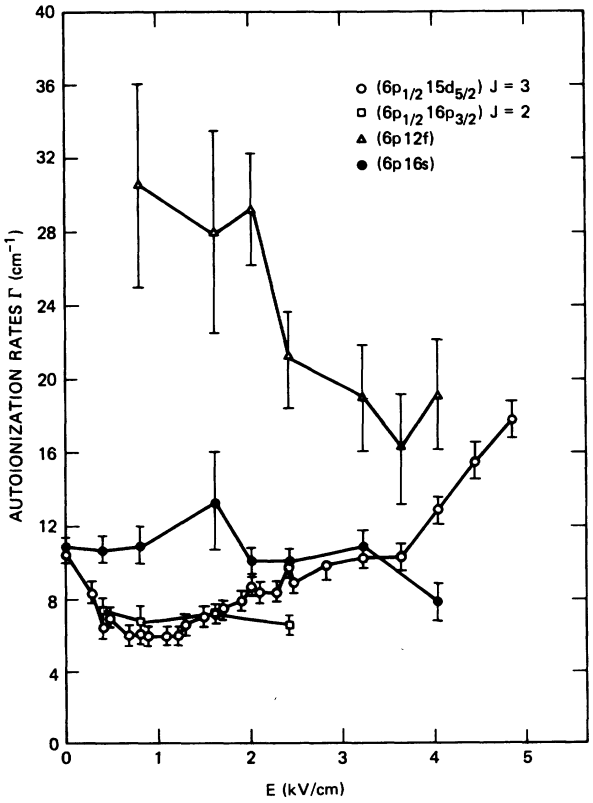

FIG. 8. Autoionization rates of $6p_{1/2}15d_{3/2}$(○), $6p_{1/2}16p_{3/2}$(□), $6p_{1/2}12f$(△), and $6p_{1/2}16s$(●) states as a function of electric field.

$(6p15d)J=3$, $(6p16p)J=2$, $6p12f$, and $6p16s$ states as a function of applied dc field. The field dependence of these widths can best be understood by considering the mixing of the bound portions of the states with other states shown in the map of Fig. 3.

The s state does not appreciably mix with any other state which can be seen from its excitation spectra as well as its independence of electric field as shown by the Stark map (Fig. 3). Its width seems to reflect this, showing little variation as a function of applied field.

The p-state component studied also shows little variation in its width; again, if we examine a typical spectrum like the one shown in Fig. 5(c) or 5(d), we see that interference effects are small, and any mixing with the d states is small.

The main component of the d state, however, shows a marked decrease in its width between 0 and ~800 V/cm. We attribute this to the mixing of this state with the sharp, and narrow, p state to its blue side. At $E \gtrsim 1$ kV/cm the p state becomes less visible in the d-state spectrum. Its width also rises back to its zero-field value, where it remains until about $E=3.5$ kV/cm. At this point the d-state spectrum shows a satellite on the blue side of the main peak due to mixing with the $6p13f$ state descending on it from above [see dashed line in Fig. 3(b)]. This mixing increases the width of the d state as shown in Fig. 8.

The f state mixes strongly with the $n=12$ hydrogenic manifold of states, as can be seen in Fig. 6. As the field strength increases so does the mixing, thereby reducing the width of the f state.

The widths of the $n=12n_1>3$ states are shown in Fig. 9 for three different field values. These field values were chosen for two different reasons. The lower limit of the field strength was determined by the oscillator strength from the $(6s6p)$ $^1P_1$ state to the $6snn_1$ states in an electric field. For fields <2 kV/cm the oscillator strengths are so small that we could not observe usable signals. The upper limit was set by where the $n=12$ manifold mixes with higher lying states and the spectra become quite complicated. For this reason the $n_1=11$ state has been ignored here, since it was difficult to observe at low fields and mixed with other states quite rapidly due to its position. Except for the two cases ($n_1=4$ at 3.69 kV/cm and $n_1=10$ at 2.05 kV/cm) discussed below, the n_1 Stark states have roughly comparable widths. Using an approximate formula[12] for the zero-field autoionization rates of the higher l states (in a.u.):

$$\Gamma_{nl}=\frac{3}{8\pi g n^3}\frac{\alpha^2 f\lambda^2}{(l-\frac{1}{2})l(l+\frac{1}{2})(l+\frac{3}{2})}, \quad (1)$$

where g is the multiplicity of the core state $(6p_{1/2})$,

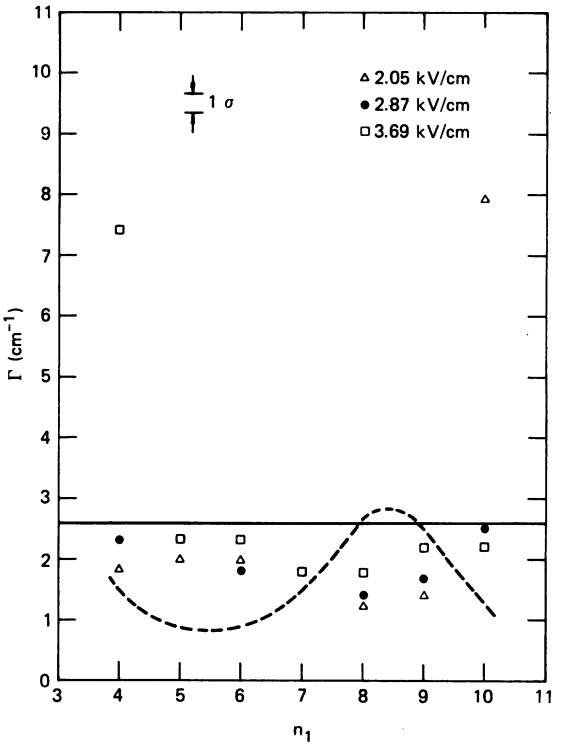

FIG. 9. Autoionization rates of the $6p_{1/2}12n_1(n_1=4-10)$ Stark states at field values of 2.05 (△), 2.87 (•), and 3.69 (□) kV/cm. The dashed curve indicate the theoretical calculations using Ref. 12 and the linear-Stark-effect approximation. The solid line indicates the unweighted average of the calculated rates.

f is the Ba^+ $6s \rightarrow 6p_{1/2}$ oscillator strength, λ is the wavelength corresponding to the Ba^+ $6s \rightarrow 6p_{1/2}$ transition, and α is the fine structure constant, we may compute the average autoionization rate for the Stark-mixed l states. Here, we took $g=3$, $f=1$, $\lambda=4935$ Å. If we take a straight average of the widths of all states that are observed to mix, i.e., $l \geq 3$, then we obtain for the average width $\bar{\Gamma}$ (in cm^{-1}):

$$\bar{\Gamma}=\tfrac{1}{8}\sum_{l=3}^{11}\Gamma_{12,l}=2.6 \quad (2)$$

which is indicated by the solid line in Fig. 9. Using a slightly more sophisticated average, we approximate the n_1 states as being hydrogenic Stark states. If we assume the linear Stark-effect approximation is valid, then we may use the parabolic basis sets $|nn_1m\rangle$[9] to describe the states. For $m=0$ states n_1 corresponds to the zero field l states. If we expand the $|nn_10\rangle$ states in terms of the zero-field $|nl0\rangle$ states, then we obtain an expression for the width of each n_1 state:

$$\Gamma_{n_1} = \frac{\sum_{l=3}^{11} |\langle 12n10|12l0\rangle|^2 \Gamma_{12,l}}{\sum_{l=3}^{11} |\langle 12n10|12l0\rangle|^2} . \tag{3}$$

In the linear Stark-effect approximation the coefficients $\langle nn_1m|nlm\rangle$ are field independent and are expressible in terms of the Wigner 3-j symbols[13]

$$\langle nn_1m|nlm\rangle = (-1)^n 1(2l+1)^{1/2} \begin{pmatrix} \frac{1}{2}(n-1) & \frac{1}{2}(n-1) & l \\ \frac{1}{2}(n-1)-n_1 & \frac{1}{2}(n-1)+n_1+m & -m \end{pmatrix} . \tag{4}$$

Substitution of Eq. (4) in Eq. (3) gives us the dashed curve in Fig. 9. Γ_{n_1} was only computed for integer values of n_1; the dashed curve was drawn through the calculated points to aid the eye in Fig. 9; therefore, the values of Γ_{n_1} should be used only for an n_1 integer. In light of the crude approximations made here we deem the agreement between experiment and theory quite good and attribute the differences between them to the inadequacy of the linear Stark-effect model in taking account of the width contributions due to mixing with other n states of large quantum defect. This shortcoming is quite apparent for the two cases mentioned above, where the disagreement is quite gross. Here the $n_1=4$ state at $E=3.69$ kV/cm is mixing strongly with the $12f$ state with a large increase in its width. Similarly, at $E=2.05$ kV/cm, the $16p$ state is crossing the $n_1=10$ state, increasing the width of the state by almost a factor of 4. Also, in using Eq. (2) to calculate the zero-field widths, we assumed that the Ba atoms autoionized to the $6s\epsilon k$ states, whereas we have recently observed that in fact an appreciable fraction of the atoms autoionize to the $5d\epsilon k$ states.[14] Therefore, we do not expect the theory to predict accurately the detailed behavior of the widths as a function of n_1. In fact, as seen in Fig. 9, the experimental values of the widths seem to oscillate with the same period and magnitude as the theory predicts, but with the opposite phase.

In summary we can say that the widths of each of the autoionizing states are affected by electric fields *only indirectly* through electric-field mixing of the discrete portions of the different Stark states. This conclusion is in basic agreement with the observations of Freeman and Bjorkland and, in the case of the higher angular-momentum states, confirms the linear Stark-effect model discussed by Jacobs and Davis.[15] There is a simple physical explanation for this. The autoionization rate is basically determined by $1/r_{12}$, which is largely a core interaction where the effects of the relatively weak static electric field are small. Thus it is not surprising that a state which does not mix with other states would have a field-free autoionization width, as is observed for the $6p_{1/2}6s$ state.

IV. DISCUSSION AND CONCLUSION

We have seen that the Stark spectroscopy of the Ba $6p_{1/2}nl$ states in the region about $n^*=12$ can be understood in terms of a simple physical picture. Basically, the electric field does not affect the excited $6p_{1/2}$ core electron. The effects on the Rydberg electron can be understood in terms of our understanding of the Stark effect for bound Rydberg levels. Singlet and triplet Rydberg states with a $6s$ core project onto the same Rydberg levels with a $6p_{1/2}$ core; however, the overlaps of the excited-core Rydberg wave functions with the single wave function differ from the overlaps with the triplet wave functions, producing different excitation spectra when the initial state in the excitation is singlet and triplet.

The effects of the electric-field mixing can be seen most clearly in the types of photoexcitation spectra obtained. In all cases the electric field seems to mix the discrete portions of the autoionizing states with little effect on the coupling to the continuum states. It is important to realize that both the initial *and* final states of the autoionizing excitation are mixed with other states by the presence of the electric field, and that any line-shape theory would have to take this into account.

These mixing effects also manifest themselves in the electric-field dependence of the energies of the different states, as shown by the Stark map, and in the field dependence of the autoionization widths of the states. An important consequence of this is that when the mixing between states is independent of electric field, as is the case for the higher-angular-momentum states in the linear-Stark-effect approximation, the autoionization rates are field independent.

In conclusion, we have studied the widths and positions of the main features of the Ba $6p_{1/2}$ Rydberg Stark states near $n^*=12$ and shown that even though the spectra are not all symmetric

lines, one can explain their general features in terms of well-understood physical arguments. Obvious extensions of this work can be realized by examining any one of the regions in the Stark map and studying it in greater detail.

Note added in proof. Aymar and Robaux[17] have labeled the $5d7d$ perturber at $W \sim 830$ cm^{-1} $^3F_2$, which agrees with the designation of Rubbmark *et al.*[11] and disagrees with the designation in this work and the work of Zimmerman *et al.*[2]

ACKNOWLEDGMENTS

We would like to acknowledge helpful discussions with W. E. Cooke and V. Jacobs. This work was supported by the Department of Energy, Office of Basic Energy Sciences.

APPENDIX

Doubly excited Rydberg autoionizing states are of particular interest since they play a major role in the dielectronic recombination of ions and electrons in plasmas, as described by Burgess.[4] The lowering of the ionization balance and the attendant radiative cooling produced by dielectronic recombination is in some cases thought to be one of the major energy losses in low-density higher-temperature plasmas. We can describe dielectronic recombination as the radiationless capture of an electron by an ion into a doubly excited Rydberg autoionizing state, followed by a stabilizing deexcitation of a core (inner) electron to a singly excited state with the emission of radiation. The Rydberg electron then cascades down to the ground state of the atom, emitting more radiation in the process. Since the radiationless capture of the electron is the inverse of the autoionization, it is clear that the dielectronic recombination rate will be determined by the autoionization rate.

An important consideration in the calculation of the recombination coefficient in a real plasma is the effect of microscopic electric fields produced by the charged particles in the plasma on the atomic system undergoing the recombination. Jacobs *et al.*[16] have considered the effect of static electric fields on the recombination rates and, using the linear-Stark-effect approximation, have found that in general one expects an enhancement of the recombination rate in the presence of electric fields.

This can perhaps be best understood by recalling that the recombination coefficient $\alpha_d(j,n-k,n)$ for an ion in the state i recombining with an electron via an autoionizing state j,n (n is the Rydberg electron principle quantum number) and stabilizing to a lower state k,n is given by[16]

$$\alpha_d(j,n-k,n)=B\sum_{lm}\frac{A_a(j,nlm-i,\epsilon_l)}{A(j,nlm)}. \qquad \text{(A1)}$$

$A_a(j,nlm-i,\epsilon_l)$ is the autoionization rate for the inverse of the radiationless capture process, and $A(j,nlm)$ is the total decay rate of the doubly excited state j,nlm via autoionization and radiative decay to all of the allowed final states. B includes a Boltzmann factor and other numerical factor which are not relevant for the purpose of this discussion. In zero field, for each l state, the ratio in the sum in Eq. (A1) approaches unity as the autoionization rate increases. For large l the field-free autoionization rates are small, and hence the ratios are small. The main contribution to the sum is from the lower l states where the ratios are relatively large. With an electric field present, it is no longer appropriate to use the $|nlm\rangle$ basis for the Rydberg electron, since all states of different l mix with one another. If we assume that the linear-Stark-effect approximation is valid, we may replace the $|nlm\rangle$ basis by $|nn_1m\rangle$ in Eq. (A1), where n_1 is the parabolic quantum number defined by Bethe and Salpeter.[9] In the approximation the parabolic basis states, and therefore their projections onto the spherical basis states, $\langle nlm|nn_1m\rangle$, are field independent. Thus the autoionization rates $A_a(j,nn_1m-i,\epsilon_l)$ can be expressed simply in terms of the field-free rates by a transformation of basis. The effect of the field is to increase the autoionization rates of the higher angular-momentum states. However, the relative increase in the ratios of the rates in Eq. (A1) for the higher angular-momentum states more than offsets the decrease of the ratios for the lower angular-momentum states, resulting in an overall enhancement of the recombination rate. This approximation is expected to be valid in electric fields where states of different n do not mix, i.e., fields $<1/n^5$.

The experimental studies of autoionizing states in electric fields have not specifically addressed this problem until now. As we have seen in Sec. III the linear-Stark-effect approximation appears to be in reasonable agreement with the data when the hydrogenic manifold of states is not mixing with states of a different manifold. Therefore, we feel that the overall enhancement of the dielectronic recombination rates in electric fields, as calculated by Jacobs *et al.*[16] is to be expected in cases where states of different n do not mix.

*Permanent address: Groupe d'Electronique dans les Gaz, Institut d'Electronique Fondamentale (Bât 220), Université de Paris Sud, 91405, Orsay, France.

[1]M. L. Zimmerman, M. G. Littman, M. M. Kash, and D. Kleppner, Phys. Rev. A 20, 2251 (1979).
[2]M. L. Zimmerman, T. W. Ducas, M. G. Littman, and D. Kleppner, J. Phys. B 11, L11 (1978).
[3]R. R. Freeman and G. C. Bjorklund, Phys. Rev. Lett. 40, 118 (1978).
[4]A. Burgess and H. P. Summers, Astrophys. J. 157, 1007 (1969).
[5]W. E. Cooke and T. F. Gallagher, Phys. Rev. Lett. 41, 1648 (1978).
[6]W. E. Cooke, T. F. Gallagher, S. N. Edelstein, and R. M. Hill, Phys. Rev. Lett. 40, 178 (1978).
[7]K. A. Safinya and T. F. Gallagher, Phys. Rev. Lett. 43, 1239 (1979).
[8]C. M. Brown and M. L. Ginter, J. Opt. Soc. Am. 68, 817 (1978).
[9]H. A. Bethe and E. E. Salpeter, *Quantum Mechanics of One- and Two-Electron Atoms* (Academic, New York, 1957).
[10]R. R. Freeman and D. Kleppner, Phys. Rev. A 14, 1614 (1976).
[11]J. R. Rubbmark, S. A. Borgstrom, and K. Bockasten, J. Phys. B 10, 421 (1977).
[12]W. E. Cooke and T. F. Gallagher, Phys. Rev. A 19, 2151 (1979).
[13]D. L. Park, Z. Phys. 159, 155 (1960).
[14]K. A. Safinya, T. F. Gallagher, and W. E. Cooke (unpublished).
[15]V. L. Jacobs and J. Davis, Phys. Rev. A 19, 776 (1979).
[16]V. L. Jacobs, J. Davis, and P. C. Kepple, Phys. Rev. Lett. 37, 1390 (1976).
[17]M. Aymar and O. Robaux, J. Phys. B 12, 531 (1979).